Journal of the Optical Society of America B
OPTICAL PHYSICS

Temporal reflection of an optical pulse from a short soliton: impact of Raman scattering

JUNCHI ZHANG,[1,*] WILLIAM DONALDSON,[2] AND GOVIND P. AGRAWAL[1]

[1]Institute of Optics, University of Rochester, Rochester, New York 14627, USA
[2]Laboratory of Laser Energetics, University of Rochester, Rochester, New York 14627, USA
*Corresponding author: jzh156@ur.rochester.edu

Received 3 May 2022; revised 9 June 2022; accepted 10 June 2022; posted 10 June 2022; published 27 June 2022

We study temporal reflection of an optical pulse from the refractive-index barrier created by a short pump soliton inside a nonlinear dispersive medium such as an optical fiber. One feature is that the soliton's speed changes continuously as its spectrum redshifts because of intrapulse Raman scattering. We use the generalized nonlinear Schrödinger equation to find the shape and spectrum of the reflected pulse. Both are affected considerably by the soliton's trajectory. The reflected pulse can become considerably narrower compared to the incident pulse under conditions that involve a type of temporal focusing. This phenomenon is explained through space–time duality by showing that the temporal situation is analogous to an optical beam incident obliquely on a parabolic mirror. We obtain an approximate analytic expression for the reflected pulse's spectrum and use it to derive the temporal version of the transformation law for the q parameter associated with a Gaussian beam.

https://doi.org/10.1364/JOSAB.462985

1. INTRODUCTION

Considerable attention has been paid recently to the reflection of optical pulses at a temporal boundary, across which the refractive index of a medium changes by a fixed amount. In some studies, the refractive index was assumed to change everywhere in the medium at the same time, a situation not easy to implement experimentally [1–7]. A more realistic situation has also been considered in which a moving temporal boundary is created, either optically or electrically, inside a dispersive medium [8–10]. When an optical pulse, moving at a different speed, arrives at the boundary, it splits into two parts with different optical spectra that move at different speeds. One part changes its speed so much that it never crosses the boundary. This is interpreted as temporal reflection. The spectral shifts of the reflected and refracted parts can be found from the momentum conservation relation [8]. When the index change at the moving boundary is large enough, the temporal analog of total internal reflection (TIR) can also occur. The TIR effect was studied earlier under the name "optical event horizon," and the frequency shift of the reflected pulse was observed experimentally using optical fibers or silicon waveguides as dispersive media [11–16].

In practice, a moving temporal boundary is created optically via the optical Kerr effect by launching a short pump pulse into a dispersive nonlinear medium such as an optical fiber. In this case, the refractive index increases by $\delta n = n_2 I(t)$ inside the region occupied by the pulse, where n_2 is the Kerr coefficient, and $I(t)$ is the intensity. As it is desirable to maintain the shape of the pulse, it helps if the pump pulse propagates as an optical soliton. To insure a high index change, the peak power of the pump pulse needs to be high. In most earlier work, the width of pump pulses is implicitly taken to be >1 ps as several higher-order effects have been ignored. In this paper, we focus on femtosecond pump pulses and ask how the process of temporal reflection is affected by the higher-order effects that influence such short solitons. The most important higher-order effect is intrapulse Raman scattering (IRS), which shifts the spectrum of the soliton toward the red side in a continuous fashion and changes its speed at the same time. As the pump pulse acts as a moving temporal boundary, the speed of the boundary does not remain constant for such short pump pulses.

The paper is organized as follows. In Section 2, we use the generalized nonlinear Schrödinger equation to derive the coupled equations that govern the evolutions of the pump pulse and the probe pulse that is reflected by the pump pulse. In Section 3, we discuss the behavior of the pump soliton with the effects of IRS included. In Section 4, we use numerical simulations to discuss temporal reflection of the probe pulse and how its magnitude depends on the frequency and width of the pump pulse. In Section 5, we discuss a new phenomenon that we call temporal focusing. Here, we stress the space–time analogy that exists between short-pulse evolution in a dispersive medium and paraxial-beam propagation in free space. We use this analogy to show that a probe pulse reflected by the Raman soliton can be focused and become much narrower than the incident pulse. In Section 6, we derive analytically the optical spectrum of the reflected pulse. We use this result to derive a transformation law

for probe pulses that appear similar to the complex q parameter used for Gaussian beams. We summarize our main results in Section 7.

2. THEORETICAL MODEL

We use optical fibers as an example of a nonlinear dispersive medium suitable for experiments on temporal reflection. It is well known that the following generalized nonlinear Schrödinger equation is an excellent model for short pulses propagating inside an optical fiber [17]:

$$\frac{\partial A}{\partial z}-\sum_{m\geq 2}\frac{i^{m+1}}{m!}\beta_m\frac{\partial^m A}{\partial t^m}=i\gamma A(z,t)\int_{-\infty}^{\infty}R(t')|A(z,t-t')|^2\mathrm{d}t', \tag{1}$$

where γ is the nonlinear parameter and β_m is the mth order dispersion parameter at the input pump pulse central frequency ω_1 and is defined $\beta_m=d^m\beta/d\omega^m|_{\omega_1}$. Fiber losses are neglected in Eq. (1) because of the relatively short lengths (<0.1 km) required for this work. The pulse's envelope $A(z,t)$ is related to the electric field as

$$E(z,t)=\frac{1}{2}\{A(z,t)\exp[i(\beta(\omega_1)z-\omega_1 t)]+\text{c.c.}\}, \tag{2}$$

where ω_1 is the central frequency of the incident pump pulse. The reduced time t is related to time in the laboratory frame t_{lab} as $t=t_{\text{lab}}-\beta_1 z$. Also, $R(t)$ is the nonlinear response function of the form

$$R(t)=(1-f_R)\delta(t)+f_R h_R(t). \tag{3}$$

The first term is the instantaneous response from the electrons, and the second term is a delayed response governed by the Raman response function $h_R(t)$. In our simulations, we used its following functional from [18]:

$$h_R(t)=(1-f_b)\frac{\tau_1^2+\tau_2^2}{\tau_1\tau_2^2}e^{-\frac{t}{\tau_2}}\sin\frac{t}{\tau_1}+f_b\frac{2\tau_b-t}{\tau_b^2}e^{-\frac{t}{\tau_b}}, \tag{4}$$

where $\tau_1=12.2$ fs, $\tau_2=32$ fs, $\tau_b=96$ fs, $f_b=0.21$, $f_R=0.245$.

To realize temporal reflection, the group-velocity difference between the pump and probe pulses should be relatively small [8]. One way to achieve this is to notice that a single-mode silica fiber has its zero-dispersion wavelength around 1310 nm, where β_2 vanishes. As β_2 has different signs on the opposite sides of this wavelength, for any wavelength of the pump, a wavelength exists on the opposite side that has the same group velocity. Figure 1 shows how the group index n_g varies with wavelength for silica fiber. The group velocity is related to it as $v_g=c/n_g$. For example, if we choose the pump's wavelength near 1500 nm, where solitons can form, the group velocity at 1145 nm will match that of the pump pulse. In practice, the central wavelength of the probe pulse should be in the range of 1145 ± 20 nm to ensure a relatively high reflectivity.

As the pump and probe have spectra that are widely separated for our choice of their wavelengths, we can consider their envelopes separately. The input pump pulse central frequency is ω_1, while the probe pulse central frequency is near the group-velocity matched frequency of ω_1, denoted as ω_2. We use frequency ω_2 to define the probe pulse envelope. Thus, the envelope A in Eq. (1) can be decomposed into the pump and the probe:

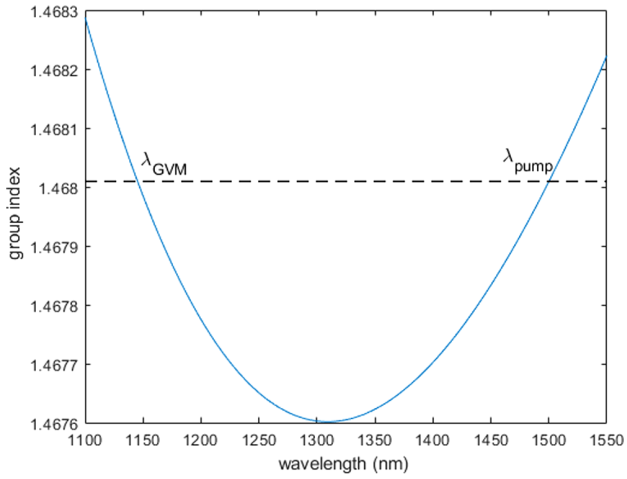

Fig. 1. Group index of a single-mode fiber. For a 1500 nm pump soliton, the group velocity matching wavelength λ_{GVM} is 1145 nm.

$$A(z,t)=A_1(z,t)+A_2(z,t)e^{i(\Delta\beta z-\Delta\omega t)}, \tag{5}$$

where $\Delta\omega=\omega_2-\omega_1$, $\Delta\beta=\beta(\omega_2)-\beta(\omega_1)-\beta_1(\omega_1)\Delta\omega$, and subscripts 1 and 2 stand for the pump and probe envelopes, respectively. Substituting the preceding form into Eq. (1) and separating the terms in the two spectral regions, we obtain the following two equations:

$$\frac{\partial A_1}{\partial z}-\sum_{m\geq 2}\frac{i^{m+1}}{m!}\beta_{m1}\frac{\partial^m A_1}{\partial t^m}=i\gamma A_1(1-f_R)(|A_1|^2+2|A_2|^2)$$
$$+i\gamma f_R\int_{-\infty}^{\infty}h_R(t')(|A_1|^2+|A_2|^2)(z,t-t')\mathrm{d}t', \tag{6}$$

$$\frac{\partial A_2}{\partial z}-\sum_{m\geq 2}\frac{i^{m+1}}{m!}\beta_{m2}\frac{\partial^m A_2}{\partial t^m}=i\gamma A_2(1-f_R)(|A_2|^2+2|A_1|^2)$$
$$+i\gamma f_R\int_{-\infty}^{\infty}h_R(t')(|A_2|^2+|A_1|^2)(z,t-t')\mathrm{d}t'. \tag{7}$$

We will use these equations to discuss temporal reflection from ultrashort pump pulses. The terms oscillating at frequencies other than those of the pump and probe were neglected in writing them. This is justified because they are the results of four wave mixing between the pump and probe, which requires a phase-matching condition that is usually not satisfied in practice.

3. RAMAN-INDUCED FREQUENCY SHIFT

When a femtosecond pulse is injected into a fiber, its spectrum is wide enough that Raman scattering can happen among its own spectral components, with the result that its spectrum shifts continuously toward the red side when it propagates in the anomalous dispersion region as a soliton. The spectral shift leads to a deacceleration of the soliton and a continuous reduction in the speed of the pulse [17]. In the moving frame we work in, this slowing down appears as a z-dependent time delay. When only the second-order dispersion is considered, the shape and width of the soliton do not change during propagation, but

its central frequency redshifts linearly with the propagation distance z [19]. In the time domain, the pulse is delayed by an amount that increases with z as z^2. This can be inferred from Eq. (6) by neglecting the terms containing A_2 and keeping only the β_2 term in the sum. If $A_1(0, t) = \sqrt{P_1}\,\mathrm{sech}(t/T_1)$, then the solution at a distance z can be written as [17]

$$A_1(z, t) = \sqrt{P_1}\,\mathrm{sech}\left(\frac{t - q_p}{T_1}\right) e^{-i\Omega_p z + i\phi_p}, \tag{8}$$

where the Raman-induced frequency and the temporal shift are given by

$$\Omega_p = -\frac{8\,T_R|\beta_{21}|z}{15\,T_1^4}, \quad q_p = \frac{4\,T_R\beta_{21}^2 z^2}{15\,T_1^4} = a z^2. \tag{9}$$

Here $T_R \approx 3$ fs is a time constant determined by the Raman response function. We introduce a coefficient $a = 4\,T_R\beta_{21}^2/(15\,T_1^4)$ to simplify the notation in the following sections. The important point relevant for this work is that the pump pulse slows down and is delayed by an amount that increases as z^2, while its shape and width remain unchanged.

4. TEMPORAL REFLECTION

To understand why the probe pulse can be reflected by the pump pulse, we simplify the probe's evolution Eq. (7). We neglect the higher-order dispersion terms in the sum, retaining only the β_2 term. We also neglect the nonlinear terms containing $|A_2|^2$ because the probe is much weaker than the pump. The resulting equation can be written in the compact form

$$\frac{\partial A_2}{\partial z} + \frac{i\beta_{22}}{2}\frac{\partial^2 A_2}{\partial t^2} = i b(z, t) A_2, \tag{10}$$

where the pump-induced change in the refractive index is given as

$$\begin{aligned} b(z, t) &= 2\gamma(1 - f_R)|A_1(z, t)|^2 \\ &\quad + \gamma f_R \int_{-\infty}^{\infty} h_R(t')|A_1(z, t - t')|^2 \mathrm{d}t' \\ &\approx \gamma(2 - f_R)|A_1(z, t)|^2. \end{aligned} \tag{11}$$

The term on the second line results from the Raman effect.

Equation (10) resembles Schrödinger's equation in quantum mechanics with $b(z, t)$ representing a barrier. Thus, our temporal-reflection problem is analogous to the scattering of a particle from a barrier in quantum mechanics. When the index change is large enough, we expect the probe pulse to be completely reflected by the pump pulse. However, as the pump pulse exhibits a Raman-induced delay, the exact quantum analog of the temporal reflection will be reflection from a non-stationary energy barrier.

To study how the Raman-induced delay of the pump pulse affects temporal reflection, we solved Eqs. (6) and (7) numerically. The dispersion parameters are $\beta_{21} = -15.7\ \mathrm{ps}^2/\mathrm{m}$, $\beta_{22} = 12.3\ \mathrm{ps}^2/\mathrm{m}$. The input pump pulse at 1500 nm has the amplitude $A_1(0, t)$ of the form in Eq. (8) with $T_1 = 100$ fs. The probe pulse's spectrum is centered at 1155 nm, 10 nm longer than the group-velocity matching wavelength of 1145 nm. Its shape corresponds to a Gaussian pulse:

$$A_2(0, t) = \exp\left[-\frac{(t - T_d)^2}{2T_2^2} - i\delta_i t\right], \tag{12}$$

where $T_2 = 1$ ps (corresponding to a width of 1.66 ps), and δ_i is the frequency difference between 1155 and 1145 nm. All simulation results in this paper use this δ_i unless stated otherwise. $T_d = 2.5$ ps is the delay of the incident probe pulse with respect to the pump pulse.

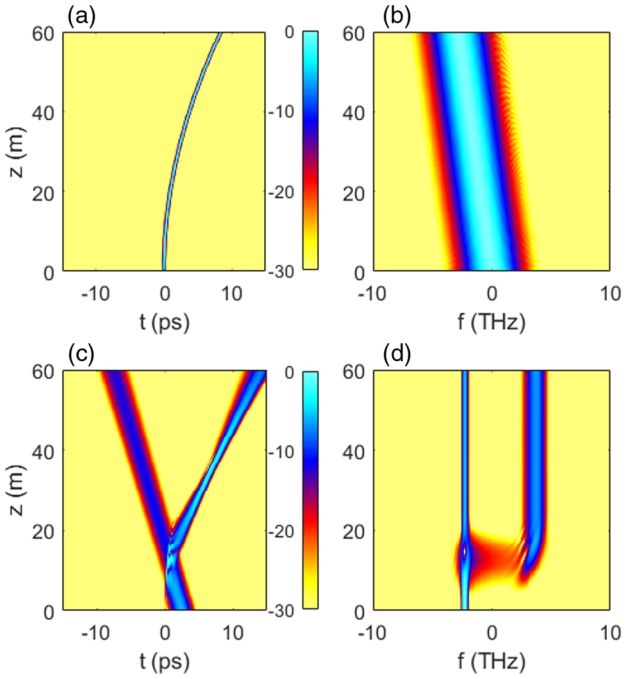

Fig. 2. Reflection of a probe pulse from a soliton that continuously redshifts. See text for parameters. (a) Pump temporal. (b) Pump spectral. (c) Probe temporal. (d) Probe spectral.

The results for a 60-m-long optical fiber are shown in Fig. 2, where we plot the evolution of the shape and spectrum of the pump (top row) and the probe (bottom row) pulses. As expected, the pump's spectrum in (b) shifts continuously toward the red side through IRS. As a result of this shift, the pump pulse slows down inside the fiber with a delay that varies as z^2, resulting in a bent trajectory in (a). In (c), the probe pulse is initially trailing the pump pulse by 2.5 ps, but it is traveling faster and catches up with the pump pulse at a distance of about 10 m. After that distance, most of its energy gets reflected by the pump pulse, while a small fraction of pulse energy is transmitted through the pump pulse and appears on its other side. The frequency of the reflected probe pulse has shifted from the incident frequency by about 6 THz, as seen in Fig. 2(d).

It is not easy to calculate analytically the reflectivity of a probe pulse from a redshifting pump soliton. However, if we make a suitable approximation, we can make some progress. The approximation consists of neglecting the spectral shift of the pump during the reflection process. In that situation, temporal reflection becomes the quantum analog of a particle scattered by a uniformly moving quantum barrier with a hyperbolic-squared shape. This problem is exactly solvable [20].

We first calculate the frequency of the reflected wave using momentum conservation or the phase-continuity relation [21]. We assume that over the duration that the probe is being reflected, the trajectory of the pump soliton can be treated as linear. Mathematically, we approximate the pump's trajectory near $z = z_0$ as

$$t_b = az^2 \approx a[z_0^2 + 2z_0(z - z_0)], \tag{13}$$

where a is a constant given in Eq. (9) and z_0 is the location where the center of the incident probe pulse hits the pump pulse. It is calculated from the quadratic equation

$$az_0^2 = T_d + \beta_{22}\delta_i z_0. \tag{14}$$

Under the linear trajectory approximation, we consider the central frequency components of the incident pulse and the reflected pulse. These two plane wave components can be written as

$$A_i \propto e^{i(\Delta\beta_i z - \delta_i t)}, \quad A_r \propto e^{i(\Delta\beta_r z - \delta_r t)}. \tag{15}$$

Along the boundary, the phase difference between the two waves should remain constant, implying the following equation:

$$\frac{d}{dz}(\Delta\beta_i z - \delta_i t_b) = \frac{d}{dz}(\Delta\beta_r z - \delta_r t_b), \tag{16}$$

with $dt_b/dz \approx 2az_0$ obtained from Eq. (13). Combined with the dispersion relation $\Delta\beta_j = \beta_{22}\delta_j^2/2$ for $j = i, r$, we obtain the reflected frequency δ_r:

$$\begin{aligned}\delta_r &= \frac{4az_0}{\beta_{22}} - \delta_i \\ &= 2\Omega_{p0}\frac{\beta_{21}}{\beta_{22}} - \delta_i,\end{aligned} \tag{17}$$

where Ω_{p0} is the Raman-induced frequency shift (RIFS) of the pump at z_0. Physically, Eq. (17) shows that the reflected pulse's frequency depends on the RIFS at the location z_0. In the preceding discussion, we considered the central frequency component of the incident probe pulse. The reflected frequency δ_r calculated from Eq. (17) is the central frequency of the reflected pulse.

Under the linear-trajectory approximation, we can use the result from [20] and write the reflectivity in the form

$$R = \left[1 + \frac{\sinh^2(\pi D/2)}{\cosh^2(\pi\sqrt{B-1}/2)}\right]^{-1}, \tag{18}$$

where $B = 8(2 - f_R)|\beta_{21}/\beta_{22}|$ and $D = (\delta_i - \delta_r)T_1$. Besides parameter B, the reflectivity depends on D, indicating that the pump 's width T_1 plays a role together with the frequency shift of the reflected pulse. The dependence of R on D is shown in Fig. 3 for three values of B, where it is shown that high reflectivity occurs for values of D roughly in the range of $-5 < D < 5$. It seems from Fig. 3 that the use of narrower pump pulses (small T_1) is preferable to enhance the reflectivity. However, a shorter pump pulse also experiences a larger RIFS, not a desirable feature in the present context.

As an example, consider a probe pulse with a Gaussian shape as in Eq. (12). If T_d is positive, the pump pulse will slow down

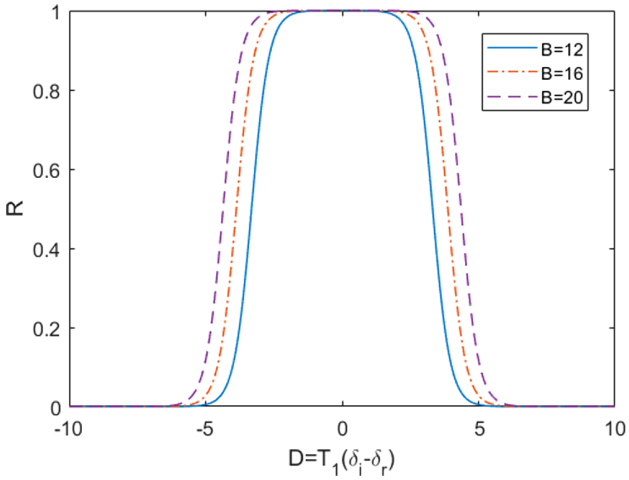

Fig. 3. Reflectivity as a function of $D = (\delta_i - \delta_r)T_1$ for three values of B based on Eq. (18).

because of the RIFS, and the pump and probe pulses will eventually collide, regardless of the frequency shift δ_i. By explicitly calculating the location z_0 from Eq. (14), we find the frequency difference $\delta_r - \delta_i$ explicitly:

$$\delta_r - \delta_i = 2\sqrt{\delta_i^2 + \frac{4a\,T_d}{\beta_{22}}}. \tag{19}$$

We can use this result in Eq. (18) to calculate the probe's reflectivity. Although this method is not rigorous, it provides a good estimate within a few percent. Its accuracy degrades for short probe pulses with a large spectral bandwidth because the result in Eq. (18) takes into account only the central frequency of the probe pulse. The linear-trajectory approximation becomes less accurate for probe pulses wider than 10 ps. In that case, the leading part of the probe pulse experiences high reflectivity with a small frequency shift, while the opposite occurs for the trailing part. The result is that the central frequency of the reflected pulse is smaller than that calculated from Eq. (17).

From Eq. (19), we can see that to maximize R, we should choose $\delta_i = 0$, i.e., the probe pulse should be group-velocity matched with the pump pulse at the input end. Additionally, we want the delay T_d to be as small as possible. Its lowest value is limited by the probe pulse's duration because the pump and probe should not overlap at the input end. The minimum value of $\delta_r - \delta_i$ is proportional to $\sqrt{a}$ or scales as $1/T_1^2$. As a result, D scale as $1/T_1$, i.e., the larger T_1 is, the higher the reflectivity becomes. However, a larger T_1 implies a smaller frequency shift. Thus, a trade-off exists between the frequency shift and the conversion efficiency. For negative values of T_d, a collision between the pump and probe pulses does not always occur. Even when a collision occurs, the reflected pulse broadens broaden rapidly, an undesirable feature in practice.

5. TEMPORAL FOCUSING

We have observed numerically a new feature for probe pulses reflected by a short soliton, whose spectrum is affected by the RIFS. When a relatively long probe pulse, initially trailing the pump, hits the pump pulse, the reflected pulse undergoes a

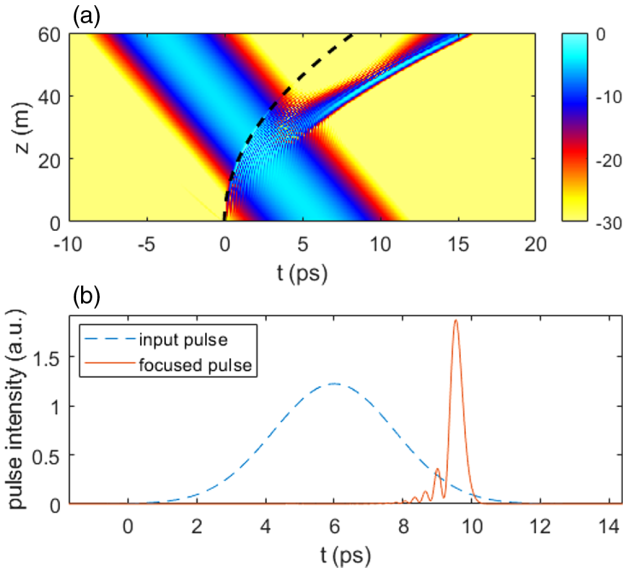

Fig. 4. Temporal focusing of a $T_2 = 2.5$ ps pulse. The pulse's temporal evolution is shown in (a). The shapes of the focused pulse (at $z = 45$ m, where the reflected pulse has the smallest width) and input pulse are given in (b).

temporal focusing phase and becomes shorter than the incident probe pulse, before broadening again, even in a medium exhibiting normal dispersion at the probe's wavelength. This behavior is shown in Fig. 4, where we display the temporal focusing for a $T_2 = 2.5$ ps pulse with delay $T_d = 6$ ps. In (a), the reflected pulse gets narrower before broadening again. This is temporal focusing. We show the reflected pulse shape at the position where it has the smallest width, and compare it with the input pulse in (b). Clearly, the reflected pulse has a much shorter width than the input pulse. The FWHM of the focused pulses is 0.4 ps, and the focusing ratio is 10.4. Temporal focusing is stronger for longer input pulses. However, there are two drawbacks. The first one is that a longer input pulse has a smaller reflectivity. The other is that when the probe pulse becomes too long, the focused pulse is distorted.

To understand the origin of temporal focusing, we make use of the well-known space–time duality between the spatial diffraction of a beam and temporal evolution of a pulse inside a dispersive medium [22–24]. This duality suggests that there must be a spatial analog of temporal focusing seen in Fig. 4. The new feature in this figure is that reflection occurs at the curved trajectory followed by the pump soliton because of the RIFS. In the spatial domain, reflection of an optical beam at a parabolic-shaped mirror corresponds to this situation. To match with our time-domain case, the bending of the mirror should occur in only one spatial dimension (see Fig. 5).

When a Gaussian beam is obliquely incident on such a partially reflecting parabolic mirror, the transmitted beam shape is not affected by the mirror, but the reflected beam is. As seen in Fig. 5, the reflected beam undergoes a focusing phase before it broadens. These features help us understand that reflection from a short soliton with a Raman-induced bent trajectory is the temporal analog of focusing by a concave mirror. From scalar diffraction theory, we know that a larger beam, when focused, can be brought down to smaller size. This explains why temporal

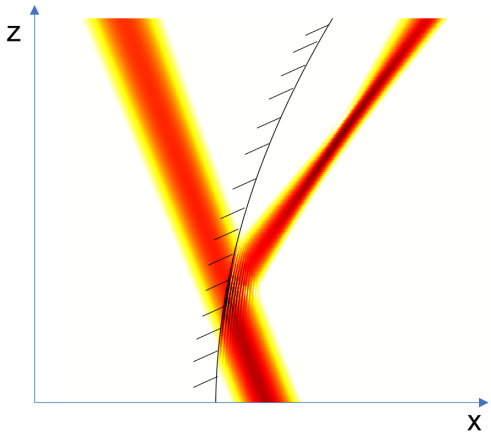

Fig. 5. Spatial analog: reflection of a Gaussian beam from a partially reflecting parabolic-shaped mirror.

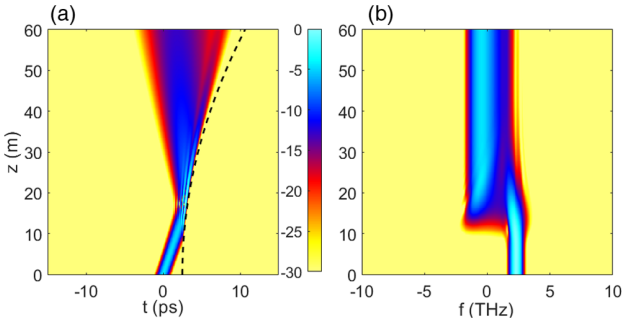

Fig. 6. Temporal defocusing induced by a pump soliton: (a) probe temporal evolution and (b) probe spectral evolution. The 1135 nm probe is a Gaussian pulse with $T_2 = 0.5$ ps and leads the pump pulse by 2.5 ps initially.

focusing is stronger for a longer input pulse. The distortion seen in Fig. 4 is the analog of the aberration that occurs when a large beam is obliquely incident on a parabolic mirror.

In Fig. 4, we consider the case where the probe pulse trails the pump pulse initially. If the incident probe leads the pump pulse and travels slower than the pump pulse, the pump's trajectory acts as a convex mirror, instead of a concave mirror. In the spatial case, the reflected beam will diverge after hitting a convex mirror. Thus, we expect the reflected pulse to become broader. An example is shown in Fig. 6. The reflected pulse has a much wider spectrum and is broadening very fast. This is consistent with our physical intuition.

6. ANALYTICAL THEORY

In this section, we develop an analytical model for the reflected pulse spectrum and use it to discuss the phenomenon of temporal focusing. We focus on the case where the probe pulse trails the pump pulse initially so that the pump's trajectory acts as a concave mirror.

The probe pulse propagates freely in a dispersive medium before and after reflection. If we include only the second-order disperison, their slowly varying envelops evolve as [17]

$$A_i(z,t)=\frac{1}{2\pi}\int_{-\infty}^{\infty}\tilde{A}_i(\omega)\exp\left(\frac{i}{2}\beta_{22}\omega^2 z-i\omega t\right)\mathrm{d}\omega, \tag{20}$$

$$A_r(z,t)=\frac{1}{2\pi}\int_{-\infty}^{\infty}\tilde{A}_r(\omega)\exp\left(\frac{i}{2}\beta_{22}\omega^2 z-i\omega t\right)\mathrm{d}\omega, \tag{21}$$

where the second equation applies after the collision of two pulses. The incident field for the Gaussian probe is used from Eq. (16). Its use allows us to calculate the inital spectrum $\tilde{A}_i(\omega)$ through a Fourier transform.

At the boundary, the reflected and incident fields satisfy the relation

$$A_r(z,t_b)=\sqrt{R}A_i(z,t_b),\quad t_b=az^2, \tag{22}$$

where the reflectivity R is given in Eq. (18). Here we have made the assumption that R does not change during the whole reflection process, and we can use its value at the center of the probe pulse. Writing $A_r(z,t_b)$ as in Eq. (21), we obtain

$$\frac{1}{2\pi}\int\tilde{A}_r(\omega)\exp\left(\frac{i}{2}\beta_{22}\omega^2 z-ia\omega z^2\right)\mathrm{d}\omega=\sqrt{R}A_i(z,az^2). \tag{23}$$

We want to deduce the spectrum of the reflected pulse from the preceding equation. This is not easy but can be done if we employ physical intuition. First, the right side is only non-zero near z_0. Second, the reflected spectrum $\tilde{A}_r(\omega)$ is centered at δ_r given by Eq. (17). Based on these observations, we can simplify the left side as

$$\begin{aligned}&\int\tilde{A}_r(\omega)\exp i(\beta_{22}\omega^2 z/2-a\omega z^2)\mathrm{d}\omega\\&=\int\tilde{A}_r(\omega)\exp i(\beta_{22}\omega^2 z/2-a\omega(2z_0z-z_0^2)-a\omega(z-z_0)^2)\mathrm{d}\omega\\&\approx e^{-ia\delta_r(z-z_0)^2}\int\tilde{A}_r(\omega)e^{ia\omega z_0^2}\exp[i(\beta_{22}\omega^2/2-2a\omega z_0)z]\mathrm{d}\omega,\end{aligned} \tag{24}$$

where we replaced ω in the term $a\omega(z-z_0)^2$ with δ_r. As the integral is now related to an inverse Fourier transform, the reflected pulse spectrum is found to be

$$\begin{aligned}\tilde{A}_r(\omega)=&F(\beta_{22}\omega^2/2-2az_0\omega)(\beta_{22}\omega-2az_0)\\&\times e^{-iaz_0^2\omega}H(\omega-2az_0/\beta_{22}),\end{aligned} \tag{25}$$

where $H(x)$ is the step function, and $F(k)$ is calculated using

$$F(k)=\sqrt{R}\int A_i(z,az^2)e^{ia\delta_r(z-z_0)^2}e^{-ikz}\mathrm{d}z. \tag{26}$$

Equation (25) provides an approximate analytic expression for the spectrum of the refelected pulse and is our main result in this section. The step function restricts the frequencies to the range $\omega>2az_0/\beta_{22}$ to ensure that the reflected pulse stays on the same side of the pump pulse as the incident pulse. To check the accuracy of Eq. (25), we compare in Fig. 7 its prediction to the numerically obtained spectrum in Fig. 2. It is evident that the analytical expression agrees quite well with the numerical results.

For an input Gaussian pulse, $A_i(z,az^2)$ can be calculated analytically. By keeping only terms up to the second order in $z-z_0$, the reflected pulse spectrum can be obtained in a closed form from Eq. (25). To simplify the notation, we define

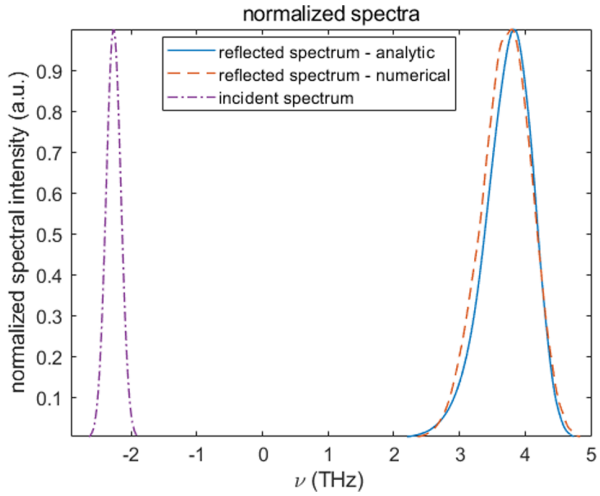

Fig. 7. Comparison of the analytically predicted and numerically simulated spectra for the reflected pulse using the parameters in Fig. 2. The analytical curve is based on Eq. (25). The incident pulse spectrum is also plotted as a reference.

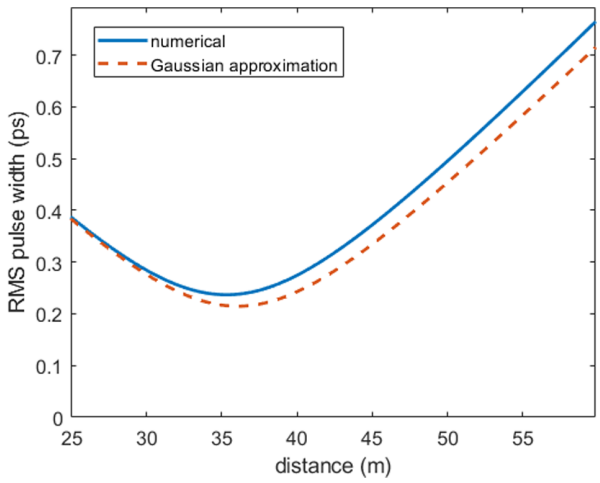

Fig. 8. Reflected pulse's RMS pulse width as it propagates. The parameters are the same as in Fig. 2. The numerical RMS pulse width obtained directly is compared with the RMS pulse width predicted by the Gaussian approximation Eq. (28).

a complex q parameter for a Gaussian pulse similar to that for a Gaussian beam and write its spectrum as

$$\tilde{A}_j(\omega)\propto\exp[-q_j(\omega-\omega_0)^2/2],\quad (j=i,r). \tag{27}$$

The reflected pulse is found to be approximately Gaussian with its central frequency at δ_r. The q parameter of the reflected pulse right after reflection is given by

$$\frac{1}{q_r(z_0)}=\frac{1}{q_i(z_0)}-\frac{8ia}{\beta_{22}^2(\delta_r-\delta_i)}, \tag{28}$$

where $q_i(z_0)=T_2^2-i\beta_{22}z_0$ is the q parameter of the probe right before reflection. This equation is similar to the transformation law for the q parameter of Gaussian beams. It shows that the space–time duality between the beams and pulses holds

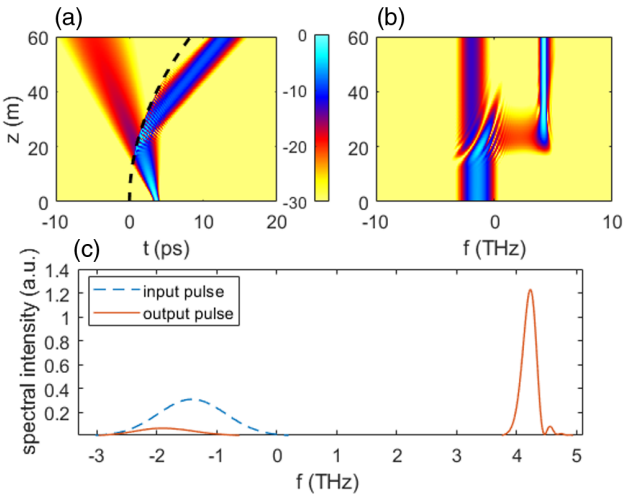

Fig. 9. Simulation result of a short probe pulse collimated by the Raman soliton. (a) Probe temporal. (b) Probe spectral. (c) Pulse spectra.

even for the q parameter. Using Eq. (28), we can find the spectral and temporal shapes of the reflected pulse. To check the accuracy of the Gaussian approximation, we compare in Fig. 8 the analytic prediction of the root mean square (RMS) width of the reflected pulse with the numerical values obtained from the simulation shown in Fig. 2. One can conclude that the Gaussian approximation works reasonably well.

Equation (28) can be used to understand the temporal focusing phenomenon discussed earlier. For a longer incident pulse, $q_i(z_0) \approx T_2^2$, and the second term of Eq. (28) gives rise to a positive imaginary part of $q_r(z_0)$. This corresponds to a negative chirp, and as it propagates, the chirp is compensated for by the dispersion, and the pulse becomes shorter than the incident pulse.

One interesting phenomenon occurs when a shorter input probe pulse is considered. In this case, the imaginary part in $q_i(z_0)$ cannot be neglected, resulting in a positive imaginary part in $1/q_i(z_0)$. This imaginary part can be cancelled by the second term in Eq. (28). In Fig. 9, we show such a result. The input pulse is a short pulse with $T_2 = 200$ fs. The frequency shift from the reference frequency $\delta_i/(2\pi) = -1.42$ THz, and the delay is 3.69 ps. In Fig. 9(a), we see that before reflection, the pulse is broadening very fast because it is short. After hitting the boundary and being reflected, the reflected pulse maintains its width without broadening. This is the temporal analog of collimation. Physically, the chirp generated during propagation gets cancelled by the reflection on a curved boundary. In the spectral domain, (c) shows that the reflected pulse has a much smaller spectral width than the incident pulse. This suggests that it may be possible to use this phenomenon to realize spectral compression.

7. CONCLUSION

In this paper, we studied temporal reflection of an optical pulse from the refractive-index barrier created by a short pump soliton inside a nonlinear dispersive medium such as an optical fiber. The new feature is that the soliton's speed changes continuously as its spectrum redshifts because of IRS. We used the generalized nonlinear Schrödinger equation, well known in the context of optical fibers, to obtain the shape and spectrum of the reflected pulse numerically and found that both are affected considerably by the soliton's Raman-induced spectral shift and temporal deceleration.

We observed that the spectrum of a reflected pulse becomes narrower under conditions that lead to a novel type of temporal focusing. This phenomenon is explained through space–time duality based on the similarity between the pulse propagation in a dispersive medium and beam propagation in the paraxial approximation. We showed that the temporal situation in our case is analogous to an optical beam incident obliquely on a parabolic mirror. Using this physical picture, we showed that temporal reflection can lead to focusing, defocusing, or collimation of optical pulses, just like a curved mirror can do so for optical beams. We were able to obtain an approximate analytic expression for the reflected pulse's spectrum and use it to derive the temporal version of the transformation law for the q parameter associated with Gaussian beams.

In this paper, we have considered fully coherent pump pulses. It is reasonable to ask how the results are affected for a partially coherent pump pulse exhibiting amplitude and phase fluctuations. As temporal reflection in our case happens inside a single-mode fiber, it is relatively insensitive to external perturbations. Phase fluctuations of the pump should not affect the results because the cross-phase modulation used in this paper does not depend on the pump's phase. Amplitude fluctuations are also not of much concern because pump pulses propagate as solitons, which are known to be stable against perturbations. As a result, the effects described in this paper should be observable in experiments.

Funding. National Science Foundation (ECCS-1933328); Department of Energy National Nuclear Security Administration (DE-NA0003856); University of Rochester; New York State Energy Research and Development Authority.

Acknowledgment. This report was prepared as an account of work sponsored by an agency of the U.S. Government. Neither the U.S. Government nor any agency thereof, nor any of their employees, makes any warranty, express or implied, or assumes any legal liability or responsibility for the accuracy, completeness, or usefulness of any information, apparatus, product, or process disclosed, or represents that its use would not infringe privately owned rights. Reference herein to any specific commercial product, process, or service by trade name, trademark, manufacturer, or otherwise does not necessarily constitute or imply its endorsement, recommendation, or favoring by the U.S. Government or any agency thereof. The views and opinions of authors expressed herein do not necessarily state or reflect those of the U.S. Government or any agency thereof.

Disclosures. The authors declare no conflicts of interest.

Data availability. Data underlying the results presented in this paper are not publicly available at this time but may be obtained from the authors upon reasonable request.

REFERENCES

1. J. Mendonça and P. Shukla, "Time refraction and time reflection: two basic concepts," Phys. Scr. **65**, 160 (2002).
2. Y. Xiao, D. N. Maywar, and G. P. Agrawal, "Reflection and transmission of electromagnetic waves at a temporal boundary," Opt. Lett. **39**, 574–577 (2014).

3. K. Tan, H. Lu, and W. Zuo, "Energy conservation at an optical temporal boundary," Opt. Lett. **45**, 6366–6369 (2020).
4. F. Morgenthaler, "Velocity modulation of electromagnetic waves," IRE Trans. Microwave Theory Tech. **6**, 167–172 (1958).
5. J. C. AuYeung, "Phase-conjugate reflection from a temporal dielectric boundary," Opt. Lett. **8**, 148–150 (1983).
6. M. F. Yanik and S. Fan, "Time reversal of light with linear optics and modulators," Phys. Rev. Lett. **93**, 173903 (2004).
7. F. Biancalana, A. Amann, A. V. Uskov, and E. P. O'Reilly, "Dynamics of light propagation in spatiotemporal dielectric structures," Phys. Rev. E **75**, 046607 (2007).
8. B. Plansinis, W. Donaldson, and G. Agrawal, "What is the temporal analog of reflection and refraction of optical beams?" Phys. Rev. Lett. **115**, 183901 (2015).
9. B. W. Plansinis, W. R. Donaldson, and G. P. Agrawal, "Cross-phase-modulation-induced temporal reflection and waveguiding of optical pulses," J. Opt. Soc. Am. B **35**, 436–445 (2018).
10. B. W. Plansinis, W. R. Donaldson, and G. P. Agrawal, "Spectral splitting of optical pulses inside a dispersive medium at a temporal boundary," IEEE J. Quantum Electron. **52**, 6100708 (2016).
11. T. G. Philbin, C. Kuklewicz, S. Robertson, S. Hill, F. Konig, and U. Leonhardt, "Fiber-optical analog of the event horizon," Science **319**, 1367–1370 (2008).
12. K. E. Webb, M. Erkintalo, Y. Xu, N. G. Broderick, J. M. Dudley, G. Genty, and S. G. Murdoch, "Nonlinear optics of fibre event horizons," Nat. Commun. **5**, 4969 (2014).
13. L. Tartara, "Frequency shifting of femtosecond pulses by reflection at solitons," IEEE J. Quantum Electron. **48**, 1439–1442 (2012).
14. C. Ciret, F. Leo, B. Kuyken, G. Roelkens, and S.-P. Gorza, "Observation of an optical event horizon in a silicon-on-insulator photonic wire waveguide," Opt. Express **24**, 114–124 (2016).
15. A. Choudhary and F. König, "Efficient frequency shifting of dispersive waves at solitons," Opt. Express **20**, 5538–5546 (2012).
16. S. Wang, A. Mussot, M. Conforti, A. Bendahmane, X. Zeng, and A. Kudlinski, "Optical event horizons from the collision of a soliton and its own dispersive wave," Phys. Rev. A **92**, 023837 (2015).
17. G. P. Agrawal, *Nonlinear Fiber Optics*, 6th ed. (Academic, 2019).
18. Q. Lin and G. P. Agrawal, "Raman response function for silica fibers," Opt. Lett. **31**, 3086–3088 (2006).
19. J. P. Gordon, "Theory of the soliton self-frequency shift," Opt. Lett. **11**, 662–664 (1986).
20. L. D. Landau and E. M. Lifshitz, *Quantum Mechanics: Non-Relativistic Theory* (Elsevier, 2013), Vol. **3**.
21. M. A. Gaafar, T. Baba, M. Eich, and A. Y. Petrov, "Front-induced transitions," Nat. Photonics **13**, 737–748 (2019).
22. B. H. Kolner, "Space-time duality and the theory of temporal imaging," IEEE J. Quantum Electron. **30**, 1951–1963 (1994).
23. R. Salem, M. A. Foster, and A. L. Gaeta, "Application of space–time duality to ultrahigh-speed optical signal processing," Adv. Opt. Photon. **5**, 274–317 (2013).
24. J. van Howe and C. Xu, "Ultrafast optical signal processing based upon space-time dualities," J. Lightwave Technol. **24**, 2649–2662 (2006).